THE JOURNAL OF PHYSICAL CHEMISTRY Letters

Letter

pubs.acs.org/JPCL

Morphological Dependence of Lithium Insertion in Nanocrystalline TiO_2(B) Nanoparticles and Nanosheets

Anthony G. Dylla, Penghao Xiao, Graeme Henkelman, and Keith J. Stevenson*

Department of Chemistry and Biochemistry, The University of Texas at Austin, Austin, Texas 78712, United States

Supporting Information

ABSTRACT: The lithium insertion behavior of nanoparticle (3-D) and nanosheet (2-D) architectures of TiO_2(B) is quite different, as observed by differential capacity plots derived from galvanostatic charging/discharge experiments. DFT+U calculations show unique lithiation mechanisms for the different nanoarchitectures. For TiO_2(B) nanoparticles, A2 sites near equatorial TiO_6 octahedra are filled first, followed by A1 sites near axial TiO_6 octahedra. No open-channel C site filling is observed in the voltage range studied. Conversely, TiO_2(B) nanosheets incrementally fill C sites, followed by A2 and A1. DFT+U calculations suggest that the different lithiation mechanisms are related to the elongated geometry of the nanosheet along the a-axis that reduces Li^+−Li^+ interactions between C and A2 sites. The calculated lithiation potentials and degree of filling agree qualitatively with the experimentally observed differential capacity plots.

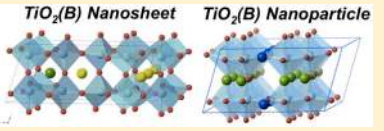

SECTION: Energy Conversion and Storage; Energy and Charge Transport

Titanium dioxide has attracted significant attention for use as a lithium ion anode material due to its specific capacity, cycling stability at high charge rates, and increased redox potential relative to graphite.[1−3] Anatase, rutile, brookite and, most recently, TiO_2(B) have been the most widely studied of the eight common polymorphs. Many of these polymorphs have been nanostructured and architecturally modified by means of particle shape control and mesoporous ordering in order to maximize both overall capacity and rate capability.[4] In particular, TiO_2(B) exhibits a high specific capacity relative to other titania polymorphs due to its low-density crystal structure. Furthermore, it can be synthesized as nanowires, nanotubes, nanoparticles, and nanosheets, which have been shown to add further capacity.[5−8] Recent efforts have focused on understanding how nanostructuring of these metal oxides affects the lithiation behavior in terms of both total storage capacity and rate capability.[9] Here, we present experimental lithiation studies and DFT+U calculations of an ultrathin nanosheet form of TiO_2(B), hereafter referred to as TiO_2(B)-NS. Galvanostatic charge/discharge experiments show unique lithiation behavior for TiO_2(B)-NS compared to nanoparticulate TiO_2(B) (TiO_2(B)-NP). DFT+U Li^+ site occupancy calculations suggest that a different Li^+ intercalation mechanism exists for 2-D nanosheet architectures of TiO_2(B) and is related to the elongated nanosheet crystal structure as well as Li^+−Li^+ repulsive interactions.

TiO_2(B) nanoparticles and nanosheets were synthesized by a previously reported method described in the Experimental Section.[7,10] Figure 1a shows TEM of TiO_2(B)-NS. The individual sheets range in size from 100 to 200 nm, are highly flexible, and have a tendency to layer on each other. High-resolution TEM (HR-TEM) of TiO_2(B)-NS in Figure 1b shows nanocrystalline domains on the surface that are consistent with the (020) lattice spacing of TiO_2(B). TEM of TiO_2(B)-NP as well as additional images of TiO_2(B)-NS are included in the Supporting Information.

Figure 2a shows X-ray diffraction (XRD) for TiO_2(B)-NS and TiO_2(B)-NP that is consistent with bulk TiO_2(B) (JCPDS# 741940). The intensity of the (020) peak at 48.6° is significantly higher for TiO_2(B)-NS than that for TiO_2(B)-NP relative to the (110) peak at 25.6°. This suggests that the TiO_2(B)-NS lay flat on surfaces, leading to a higher relative intensity of the (020) facet compared to other peaks, which is consistent with previous reports.[10] Raman spectroscopy is a useful tool for characterizing titania phases due to the highly variable local bonding structure of the different polymorphs as well as being able to determine noncrystalline phases that may be unobservable in XRD analysis.[11,12] The TiO_2(B)-NP Raman spectrum in Figure 2b is consistent with that of bulk TiO_2(B) (see Supporting Information) and previous reports.[13] The TiO_2(B)-NS spectrum is quite similar to both the TiO_2(B)-NP and bulk spectra from 200 to 700 cm^{-1} but deviates significantly below 200 cm^{-1} as several of the low-energy Ti−O−Ti and O−Ti−O torsional modes are absent at 140 and 150 cm^{-1}. The absence of peaks may be due to dimensional constraint of the 2-D architecture causing these modes to be inaccessible. Through careful synthesis and characterization of the materials, we are confident in the phase purity of the TiO_2(B)-NS and -NP materials. TiO_2(B) is a kinetic phase of titania, and anatase impurities are often present that can make further interpretation of electrochemical data more difficult.[14,15]

Bruce and co-workers have pioneered much of the work regarding lithiation of TiO_2(B) and have shown that nanostructuring significantly increases the specific capacity due to

Received: June 13, 2012
Accepted: July 16, 2012

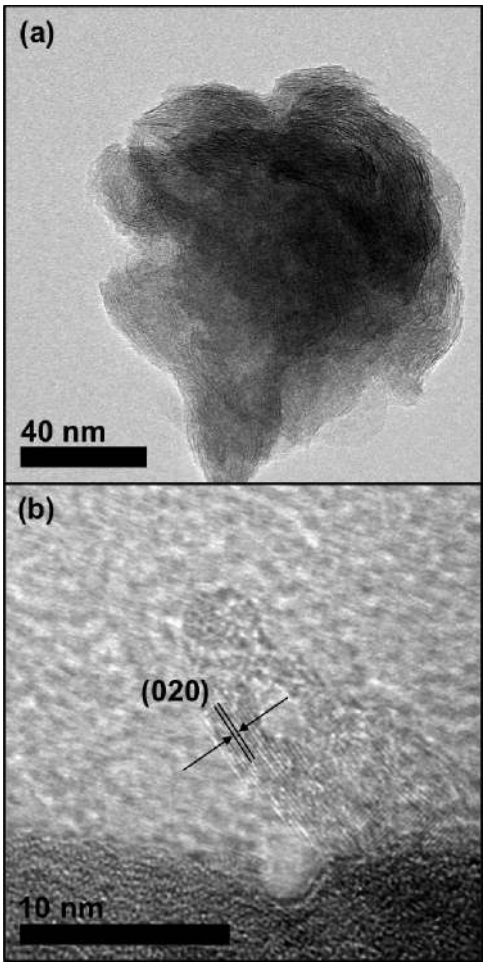

Figure 1. TEM (a) and HR-TEM (b) images of TiO_2(B) nanosheets.

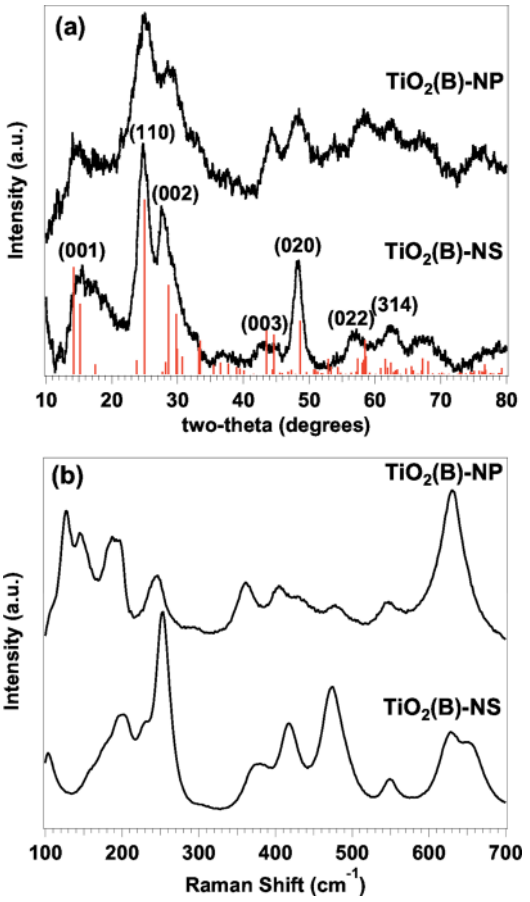

Figure 2. XRD (a) and Raman (b) of TiO_2(B) nanosheets and nanoparticles. Vertical lines represent ideal TiO_2(B) diffraction (JCPDS# 741940).

relaxed surface lithiation energetics in these high-surface-area materials. In particular, they found that the nanotube and nanoparticle forms of TiO_2(B) offer the highest overall capacity along with the best rate performance.[7] Figure 3a shows galvanostatic charge/discharge curves for both TiO_2(B)-NS and -NP upon slow rate cycling (25 mA/g, 0.07 C) after the third cycle. Both TiO_2(B)-NP and -NS show a sloping profile characteristic of nanostructured Li^+ insertion materials with the majority of the lithiation occurring below 1.7 V versus Li/Li^+.[1] The specific capacity was 259 and 275 mAh/g for TiO_2(B)-NP and TiO_2(B)-NS, respectively, after the third cycle. The specific capacity for TiO_2(B)-NP is similar to what is recently reported by Ren and co-workers.[7] A recent report by Liu and co-workers on the lithiation of porous TiO_2(B) nanosheets demonstrated a first charge specific capacity of 332 mAh/g at 0.1 C but did not mention capacity after multiple cycles at that charge rate.[8]

Differential capacity plots (dC/dV) are often constructed from galvanostatic charging curves in order to more clearly see the Li^+ insertion/deinsertion redox behavior of an electrode, particularly when the plateaus are not obvious, as is the case for many nanomaterials. Figure 3b shows dC/dV plots for both TiO_2(B)-NP and -NS morphologies. The reduction (lithiation of TiO_2(B)) portion of the dC/dV plot for TiO_2(B)-NP shows one large, well-defined peak at 1.55 V, a small shoulder at 1.5 V, followed by a capacitive-like region extending from 1.4 to 1.0 V. In contrast, TiO_2(B)-NS shows a single peak centered near 1.5 V that is surrounded by a broad, capacitive-like envelope stretching from 1.8 to 1.0 V. The nature of the sloping galvanostatic profile and consequent broad reduction peak in the dC/dV plot of TiO_2(B)-NS is likely due to the increased influence of surface effects that would change the overall charging behavior for a high-surface-area 2-D nanostructured material.[16] The broad charge/discharge profile could also be explained in terms of pseudocapacitive charging, which is a surface-specific redox process. The extent of charge (Δq) is dependent upon the change in voltage (ΔV), and thus, the total charge passed, $d(\Delta q)/d(\Delta V)$, is the equivalent of capacitance and gives rise to the sloping galvanostatic profiles.[17] This Li^+ insertion mechanism is consistent with what one would expect for a nanosheet structure where surface charging would be the main contributor to the total charge capacity. In contrast, while the TiO_2(B)-NP galvanostatic profile is also sloped, the dC/dV plot reveals more discrete Li^+ insertion/deinsertion redox behavior. These effects can be difficult to elucidate because defining the surface bonding structure and Li^+ binding sites of nanomaterials is typically inaccessible via traditional characterization methods. DFT+U calculations were performed to determine a mechanism that explains the different charging behavior observed for TiO_2(B)-NP and -NS. Figure 4 presents the DFT+U determined Li^+ site occupancy within the TiO_2(B) structure as a function of voltage for 3-D (nanoparticles) and 2-D (nanosheets) structures along with dC/dV plots with an overlay of the DFT+U derived voltages and relative Li^+ concentrations. The U value for Ti is taken from a study of rutile TiO_2, where it was adjusted to match the experimental

dx.doi.org/10.1021/jz300766a | J. Phys. Chem. Lett. 2012, 3, 2015−2019

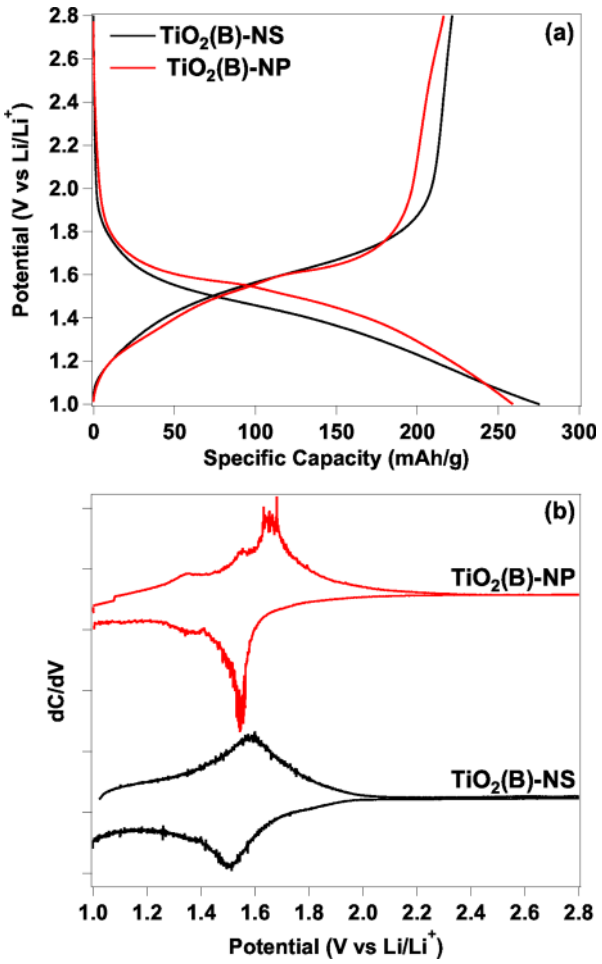

Figure 3. Third cycle galvanostatic charge/discharge curves (a) and differential capacity plots (b) for TiO_2(B) nanosheets and nanoparticles at a charge/discharge rate of 25 mA/g.

excitation energy from a localized state at an oxygen vacancy to the conduction band; the same *U* value has been used to study Li ion diffusion in anatase.[18] Although DFT+*U* correctly describes the localization of 3d electrons, it overestimates the lattice constants of TiO_2(B) by up to 3.7%. Good agreement with experiment can be obtained with the HSE06 functional (see Table S.I.4 Supporting Information), which includes a portion of exact exchange and does not have any system-specific parameters. Li ion binding energies are weaker using HSE06 than DFT+U, by −0.36 eV at the A1 site in $LiTiO_2$ and −0.29 eV at the A2 site in $Li_{0.5}TiO_2$. We used the average value, −0.32 eV, to correct our DFT+*U* values in larger cells, to match the HSE06 functional. Theoretical charge/discharge voltages are calculated as the energy to insert/remove Li atoms from the most favorable binding site, assuming the transfer of one electron per Li ion.

TiO_2(B) has a monoclinic *C*2/*m* structure with an open channel parallel to the *b*-axis that sits between axial oxygens. The unit cell contains 8 Ti sites and 10 Li^+ sites, giving a theoretical capacity of 1.25 Li^+/Ti (∼420 mAh/g). Li^+ can bind to three unique sites within the crystal; four A1 and four A2 sites sit near equatorial and axial oxygens in the titania octahera, respectively, and two C sites lie in the open channel along the *b*-axis. Two distinct Li^+ insertion mechanisms are presented here, and we start with the case of TiO_2(B)-NP.

In the dilute limit (no interaction between Li^+), the C site (designated as yellow) is the most energetically favorable binding site, with a binding energy of 1.55 eV. Li^+ binding to the A2 (designated as green) and A1 sites (designated as blue) is 0.01 and 0.22 eV weaker than that to the C site, respectively. Given the uncertainty in DFT calculations, the C and A2 sites are expected to be equally occupied in the dilute limit. Once an A2 site is occupied by a single Li^+, the binding energy of another Li^+ to the neighboring sites is affected dramatically. Li^+ binding to the nearest A2 and A1 site increases to 1.73 and 1.57 eV, respectively. This stabilizing feature is similar to that observed for $LiFePO_4$; multiple Li^+ sharing an electron localized on a transition-metal center strengthens the Coulomb attraction.[19] The nearest C site is then unstable due to the repulsion of Li^+ at the A2 sites.[20,21] Therefore, when the voltage reaches 1.54 V, the A2 sites and a dilute concentration of A1 sites will be filled. As the voltage decreases to 1.5 V, Li^+ fills alternating A1 sites, giving a Li^+/Ti ratio of 0.75. The remaining A1 sites fill at 0.98−0.56 V, reaching Li^+/Ti = 1.0. With all A2 sites occupied, a new site then becomes stable in the open channel along the *b*-axis at the midpoint between two neighboring C. These sites, designated as C′, are less stable

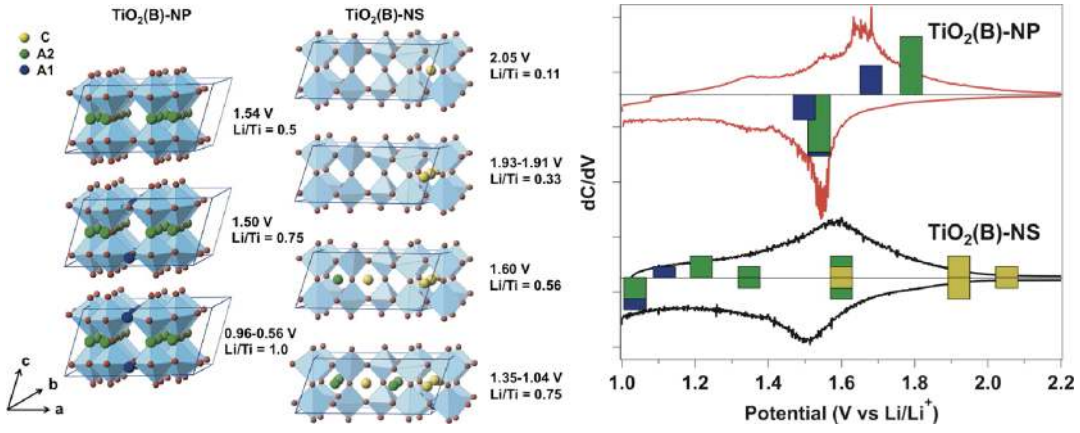

Figure 4. DFT+*U* calculated site occupancies and potentials as a function of Li^+ concentration in TiO_2(B)-NS and -NP (left) with d*C*/d*V* plots indicating DFT+*U* derived voltages and relative Li^+ site filling (right). The calculated peak splitting, particularly apparent in the NP case, is due to the response of the material Li^+ insertion, resulting in a different energy to insert Li^+ into the delithiated material as compared to the removal of Li^+ from the lithiated material. Blue, green, and yellow spheres and histogram bars correspond to A1, A2, and C sites, respectively.

dx.doi.org/10.1021/jz300766a | *J. Phys. Chem. Lett.* 2012, 3, 2015−2019

than A1 sites and are the last sites to be filled at voltages below 0.19 V (not shown). These calculations are in qualitative agreement with the experimental dC/dV plot for TiO_2(B)-NP (Figure 3b). The well-defined redox peak observed at ∼1.55 V is assigned to the initial filling of all A2 sites along with a small amount of A1 sites, and the shoulder at 1.5 V is assigned to the half filling of A1 sites. The capacitive-like region below 1.4 V may have to do with nanoscale or surface effects.[1] Additionally, the theory qualitatively predicts the experimentally observed redox peak splitting during the delithiation (oxidation) process. More Li^+−Ti Coulomb interactions are expected in the fully lithiated TiO_2(B) structure, and therefore, the delithiation process should occur at higher potentials (overpotentials) relative to lithiation due to an energetic penalty for deinserting lithium ions.

For the case of TiO_2(B)-NS, the loss of periodicity along the *b*-axis reduces the chance for localized electron sharing, and the *a*-axis of the unit cell increases from 12.5 Å for the TiO_2(B)-NP to 13.6 Å for the calculated stable TiO_2(B)-NS structure (see Supporting Information). The TiO_2(B)-NS thickness of the model structure was derived from AFM measurements previously reported by Xiang and co-workers. The A2 sites shift away from the C sites, with two adjacent A2 sites merging into one as the crystal structure is lengthened along the *a*-axis. Having the A2 site farther away from the C site alleviates repulsion between Li^+ and makes C site filling energetically more favorable for TiO_2(B)-NS. These shifts cause the site preference in TiO_2(B)-NS to be quite different from that in the TiO_2(B)-NP system. The theoretical voltages of the site filling for TiO_2(B)-NS are shown in Figure 4 (left) along with an overlay of the DFT+U derived voltages and relative Li^+ concentrations on the dC/dV plot (right). The first C sites are filled between 2.05 and 1.91 V, giving Li^+/Ti = 0.25. An A2 site is filled along with another C site at 1.6 V, followed by further A2 and A1 site filling between 1.35 and 1.04 V, with a final Li^+/Ti ratio of 0.75. This incremental site filling is qualitatively consistent with the dC/dV plot for TiO_2(B)-NS, which shows a single broad peak at 1.5 V. Furthermore, the experimentally determined capacity at 1.0 V for both TiO_2(B)-NP and -NS (∼265 mAh/g) is quite close to the value determined by DFT+U (Li^+/Ti = 0.75 = 251 mAh/g) despite the difference in apparent lithiation mechanisms. The DFT+U calculated delithiation (oxidation) process for TiO_2(B)-NS shows some redox peak splitting at low potentials, but at higher potentials, redox peak splitting is not observed. The loss of localized electron sharing in the TiO_2(B)-NS structure decreases Coulomb interactions at high Li^+ concentrations, and therefore, there is no energetic penalty for delithiation relative to lithiation.

The DFT calculated Li^+ site occupation of TiO_2(B) has been previously reported by others. In a combined DFT and experimental study, Islam and co-workers found C site binding to be preferential, followed by A2 and A1. However, speculation of anatase impurities mixed with the TiO_2(B) used in this study may have led to an incorrect interpretation of the data.[22] In this and other theoretical studies, the energy penalty (+U) was not included in the calculations.[20,23,24] Morgan and co-workers recently showed that DFT alone is inadequate to describe Li^+ binding in anatase because of the delocalization of 3d electrons over all Ti centers.[18] Only by adding the energy penalty that forces 3d electrons to localize at Ti centers does the theory predict the expected Li^+ site occupation behavior.

Here, we have shown the first direct study of the influence of dimensional confinement effects on lithiation of nanocrystalline TiO_2(B). By comparing the experimental and calculated Li^+ insertion into 3-D and 2-D architectures of TiO_2(B), we found that while both architectures have essentially the same capacity when lithiated at 1.0 V under slow charging conditions, the inherent lithiation mechanisms appear to be quite different due to the relaxed structure of TiO_2(B)-NS that cause Li^+−Li^+ repulsion in neighboring A2 and C sites to be reduced. In ongoing work, we are performing rate-dependent lithiation studies as well as in situ vibrational spectroscopy and high-resolution electron microscopy studies to further elucidate the lithiation/delithiation kinetics of this important titania polymorph.

EXPERIMENTAL METHODS

TiO_2(B) nanoparticles were synthesized as previously reported by Ren and co-workers.[7] Ti (103 mg, 99.7%, 100 mesh from Aldrich) was added to 10 mL of H_2O_2 (30%, Fisher) and 3.4 mL of NH_4OH (29.4%, Fisher). This mixture was stirred in an ice bath until all of the Ti metal had dissolved. Then, 245 mg of glycolic acid (Fluka) was added, and the mixture was heated to 80 °C to drive off excess ammonia and hydrogen peroxide. The resultant yellow gel product confirmed the formation of the Ti−glycolate complex. The gel product was dissolved in 5.7 mL of H_2O (18 MΩ cm Nanopure Barnstead), and 0.235 mL of H_2SO_4 (97.3%, Fisher) was added to form the hydrogen titanate precursor of TiO_2(B). The red solution was placed in a Teflon reactor inside of a steel acid digestion bomb (Parr Instruments), heated at 165 °C for 40 min, and cooled quickly in an ice bath. The resultant TiO_2(B) nanoparticles were washed several times with ethanol and water, centrifuged, and dried overnight at 60 °C. Finally, the powder was heated slowly (1 °C/min) to 300 °C to remove any remaining organic residues from the nanoparticle surface. TiO_2(B) nanosheets were synthesized using a previous method reported by Xiang et al.[10] Here, 1 mL of $TiCl_3$ (Alfa Aesar, 20% in 3% HCl) and 1 mL of H_2O were added to 30 mL of ethylene glycol (Aldrich) in a 100 mL round-bottom flask. This mixture was slowly stirred at 150 °C for 3 h open to air. The off-white-colored product was washed several times with ethanol and water followed by centrifugation and drying overnight at 60 °C. Finally, the powder was vacuum-annealed at 250 °C for 4 h to remove surface-adsorbed ethylene glycol.

The materials were characterized by TEM (Jeol 2010F operated at 200 kV), XRD (Rigaku Spider, Cu Ka radiation, λ = 1.5418 Å), and Raman (Renishaw InVia microscope with a 514 nm Ar^+ laser operated below 4 mW). Galvanostatic measurements were performed on an Arbin Instruments BT-2043 battery cycler operated between 1.0 and 2.8 V versus Li/Li^+ at a 25 mA/g charge rate. Coin cells were constructed inside of an MBraun glovebox with <0.1 ppm H_2O and <1.0 ppm O_2. The working electrode slurry (85% active material, 10% Super P carbon, 5% PVDF binder) was cast onto Cu current collectors and dried overnight under vacuum at 80 °C. Li metal served as the counter and reference electrodes, and 1.0 M $LiPF_6$ in EC/DMC (1:1) v/v (Novolyte Technologies) was used as the electrolyte.

All calculations were performed with the Vienna ab initio simulation package (VASP) at the GGA+U level of theory.[25,26] The functional for electron exchange and correlation was chosen as PW91, and the effective U value for Ti, $U_{eff} = U - J$, was set to 4.2 eV.[18,27] Core electrons were described in the

dx.doi.org/10.1021/jz300766a | J. Phys. Chem. Lett. 2012, 3, 2015−2019

projected augmented wave formalism.[28] Valence electrons were described by a plane wave basis set with an energy cutoff of 325 eV.[29,30] Spin polarization was applied for all calculations. Lattice constants were relaxed whenever the lithium concentration changed. For the HSE06 calculations, a harder oxygen pseudopotential was used, and the energy cutoff was increased to 400 eV correspondingly.

■ ASSOCIATED CONTENT

Supporting Information

Raman spectra of bulk TiO_2(B), TEM of TiO_2(B)-NP and additional TEM of TiO_2(B)-NS, additional differential capacity plots at faster charge rates, a side view of the calculated TiO_2(B)-NS crystal structure, and cell parameters for the calculated bulk and nanosheet structures. This material is available free of charge via the Internet at http://pubs.acs.org.

■ AUTHOR INFORMATION

Corresponding Author

*E-mail: stevenson@cm.utexas.edu.

Notes

The authors declare no competing financial interest.

■ ACKNOWLEDGMENTS

This material is based upon work supported as part of the program "Understanding Charge Separation and Transfer at Interfaces in Energy Materials (EFRC:CST)", an Energy Frontier Research Center funded by the U.S. Department of Energy, Office of Science, Office of Basic Energy Sciences under Award Number DE-SC0001091.

■ REFERENCES

(1) Wagemaker, M.; Mulder, F. M. Properties and Promises of Nanosized Insertion Materials for Li-Ion Batteries. *Acc. Chem. Res.* **2012**, DOI: 10.1021/ar2001793.

(2) Myung, S.-T.; Takahashi, N.; Komaba, S.; Yoon, C. S.; Sun, Y.-K.; Amine, K.; Yashiro, H. Nanostructured TiO_2 and Its Application in Lithium-Ion Storage. *Adv. Funct. Mater.* **2011**, *21*, 3231−3241.

(3) Bruce, P. G.; Scrosati, B.; Tarascon, J.-M. Nanomaterials for Rechargeable Lithium Batteries. *Angew. Chem., Int. Ed.* **2008**, *47*, 2930−2946.

(4) Liu, J.; Liu, X.-W. Two-Dimensional Nanoarchitectures for Lithium Storage. *Adv. Mater.* **2012**, DOI: 10.1002/adma.201104993.

(5) Armstrong, A. R.; Armstrong, G.; Canales, J.; Garcia, R.; Bruce, P. G. Lithium-Ion Intercalation into TiO_2 B Nanowires. *Adv. Mater.* **2005**, *17*, 862−865.

(6) Armstrong, G.; Armstrong, A. R.; Canales, J.; Bruce, P. G. Nanotubes with the TiO_2-B structure. *Chem. Commun.* **2005**, 2454.

(7) Ren, Y.; Bruce, P. G. Nanoparticulate TiO_2(B): An Anode for Lithium-Ion Batteries. *Angew. Chem., Int. Ed.* **2012**, 1−5.

(8) Liu, S.; Jia, H.; Han, L.; Wang, J.; Gao, P.; Xu, D.; Yang, J.; Che, S. Nanosheet-Constructed Porous TiO_2-B for Advanced Lithium Ion Batteries. *Adv. Mater.* **2012**, *24*, 3201−3204.

(9) Wang, J.; Polleux, J.; Lim, J.; Dunn, B. Pseudocapacitive Contributions to Electrochemical Energy Storage in TiO_2 (Anatase) Nanoparticles. *J. Phys. Chem. C* **2007**, *111*, 14925−14931.

(10) Xiang, G.; Li, T.; Zhuang, J.; Wang, X. Large-Scale Synthesis of Metastable TiO_2(B) Nanosheets with Atomic Thickness and Their Photocatalytic Properties. *Chem. Commun.* **2010**, *46*, 6801−6803.

(11) Beuvier, T.; Richard-Plouet, M.; Brohan, L. Accurate Methods for Quantifying the Relative Ratio of Anatase and TiO_2(B) Nanoparticles. *J. Phys. Chem. C* **2009**, *113*, 13703−13706.

(12) Ben Yahia, M.; Lemoigno, F.; Beuvier, T.; Filhol, J.-S.; Richard-Plouet, M.; Brohan, L.; Doublet, M.-L. Updated References for the Structural, Electronic, and Vibrational Properties of TiO_2(B) Bulk Using First-Principles Density Functional Theory Calculations. *J. Chem. Phys.* **2009**, *130*, 204501.

(13) Kobayashi, M.; Petrykin, V. V.; Kakihana, M.; Tomita, K.; Yoshimura, M. One-Step Synthesis of TiO_2(B) Nanoparticles from a Water-Soluble Titanium Complex. *Chem. Mater.* **2010**, 1−4.

(14) Kavan, L.; Kalbáč, M.; Zukalová, M.; Exnar, I.; Lorenzen, V.; Nesper, R.; Graetzel, M. Lithium Storage in Nanostructured TiO_2 Made by Hydrothermal Growth. *Chem. Mater.* **2004**, *16*, 477−485.

(15) Zukalova, M.; Kalbac, M.; Kavan, L.; Exnar, I.; Graetzel, M. Pseudocapacitive Lithium Storage in TiO_2(B). *Chem. Mater.* **2005**, *17*, 1248−1255.

(16) Liu, J.; Chen, J. S.; Wei, X.; Lou, X. W.; Liu, X.-W. Sandwich-Like, Stacked Ultrathin Titanate Nanosheets for Ultrafast Lithium Storage. *Adv. Mater.* **2010**, *23*, 998−1002.

(17) Conway, B. E. *Electrochemical Supercapacitors*; Scientific Fundamentals and Technological Applications; Kluwer Academic/Plenum Publishers: New York, 1999; pp 221−241.

(18) Morgan, B. J.; Watson, G. W. GGA+ U Description of Lithium Intercalation Into Anatase TiO_2. *Phys. Rev. B* **2010**, *82*, 144119.

(19) Dathar, G. K. P.; Sheppard, D.; Stevenson, K. J.; Henkelman, G. Calculations of Li-Ion Diffusion in Olivine Phosphates. *Chem. Mater.* **2011**, *23*, 4032−4037.

(20) Koudriachova, M. V. Enhanced Li-Transport on the Nanoscale: TiO_2-B Nanowires. *J. Nano Res.* **2010**, 1−8.

(21) Okumura, T.; Fukutsuka, T.; Yanagihara, A.; Orikasa, Y.; Arai, H.; Ogumi, Z.; Uchimoto, Y. Electronic and Local Structural Changes with Lithium-Ion Insertion in TiO_2-B: X-ray Absorption Spectroscopy Study. *J. Mater. Chem.* **2011**, *21*, 15369.

(22) Armstrong, A. R.; Arrouvel, C.; Gentili, V.; Parker, S. C.; Islam, M. S.; Bruce, P. G. Lithium Coordination Sites in Li_xTiO_2(B): A Structural and Computational Study. *Chem. Mater.* **2010**, *22*, 6426−6432.

(23) Koudriachova, M. V. Role of the Surface in Li Insertion into Nanowires of TiO_2-B. *Surf. Interface Anal.* **2010**, *42*, 1330−1332.

(24) Dalton, A. S.; Belak, A. A.; Van der Ven, A. Thermodynamics of Lithium in TiO_2(B) from First Principles. *Chem. Mater.* **2012**, *24*, 1568−1574.

(25) Kohn, W.; Becke, A. D.; Parr, R. G. Density Functional Theory of Electronic Structure. *J. Phys. Chem.* **1996**, *100*, 12974−12980.

(26) Kohn, W. Self-Consistent Equations Including Exchange and Correlation Effects. *Phys. Rev.* **1965**, *140*, A1133−A1138.

(27) Perdew, J. P. In *Electronic Structure of Solids*; Ziesche, P., Eschrig, H., Eds. Akademie Verlag: Berlin, Germany, 1991; pp 11−20.

(28) Kresse, G. From Ultrasoft Pseudopotentials to the Projector Augmented-Wave Method. *Phys. Rev. B* **1999**, *59*, 1758−1775.

(29) Kresse, G.; Furthmüller, J. Efficiency of Ab-Initio Total Energy Calculations for Metals and Semiconductors Using a Plane-Wave Basis Set. *Comput. Mater. Sci.* **1996**, *6*, 15−50.

(30) Kresse, G.; Furthmüller, J. Efficient Iterative Schemes for Ab Initio Total-Energy Calculations Using a Plane-Wave Basis Set. *Phys. Rev. B: Condens. Matter* **1996**, *54*, 11169−11186.

■ NOTE ADDED AFTER ASAP PUBLICATION

This paper was published ASAP on July 18, 2012. Figure 4 caption was updated. The revised paper was reposted on July 20, 2012.